Decentralised control method for DC microgrids with improved current sharing accuracy

Jie Yang[1] ✉, Xinmin Jin[1], Xuezhi Wu[1], Pablo Acuna[2], Ricardo P. Aguilera[3], Thomas Morstyn[2], Vassilios G. Agelidis[4]

[1]National Active Distribution Network Technology Research Center, Beijing Jiaotong University, Beijing, People's Republic of China
[2]School of Electrical Engineering and Telecommunications, University of New South Wales, Sydney, Australia
[3]School of Electrical, Mechanical and Mechatronic Systems, University of Technology Sydney, Sydney, Australia
[4]Electric Power and Energy (CEE), Department of Electrical Engineering, Technical University of Denmark, Kgs. Lyngby, Denmark
✉ E-mail: jieyang@bjtu.edu.cn

Abstract: A decentralised control method that deals with current sharing issues in dc microgrids (MGs) is proposed in this study. The proposed method is formulated in terms of 'modified global indicator' concept, which was originally proposed to improve reactive power sharing in ac MGs. In this work, the 'modified global indicator' concept is extended to coordinate dc MGs, which aims to preserve the main features offered by decentralised control methods such as no need of communication links, central controller or knowledge of the microgrid topology and parameters. This global indicator is inserted between current and voltage variables by adopting a virtual capacitor, which directly produces an output current sharing performance that is less relied on mismatches of the multi-bus network. Meanwhile, a voltage stabiliser is complementary developed to maintain output voltage magnitude at steady state through a shunt virtual resistance. The operation under multiple dc-buses is also included in order to enhance the applicability of the proposed controller. A detailed mathematical model including the effect of network mismatches is derived for analysis of the stability of the proposed controller. The feasibility and effectiveness of the proposed control strategy are validated by simulation and experimental results.

1 Introduction

The concept of microgrids (MGs) has been introduced in order to provide optimal and reliable operation to power systems by integrating and utilising distributed energy resources (DERs) [1]. According to the voltage type of the main bus, MGs can be distinguished as ac and dc MGs [2, 3]. Although goals are specific to each type of MGs, when natively dc loads are connected, the dc MGs have become popular recently thanks to its own advantages [4, 5]. Dc MGs can achieve higher efficiency by eliminating redundant power conversion stages traditionally used when distributed generations (DGs) such as photovoltaic (PV) modules and batteries are linked through the same bus voltage level along the MG. Furthermore, since reactive power and skin effect are not present, dc MGs offer higher power quality than MGs inserted into ac power systems [6]. Consequently, the operation of dc MGs and their coordinated control system has an increasing practical value.

For the purpose of maintaining a high quality and reliable electrical power system, the coordinated control system which governs the DGs is a key element for both ac and dc MGs. The main objective of a coordinated control system is to prevent over stressing of any energy source and properly distribute the total power load to each DG in proportion to their rated powers [7, 8]. To realise this, the so called droop control which employs own electrical parameters as global indicators is widely applied in MG systems due to its decentralised characteristic [9–12]. For ac MGs, the classical global indicators, namely frequency and voltage, are applied in *P-f* and *Q-V* droop controllers in order to provide power sharing. In addition, the reactive power sharing is improved by taking into account a modified global indicator, change rate of the voltage [13, 14]. While for dc MGs, the main difference from ac MGs is that its I–V droop control has an inherent virtual resistance feature, which is employed directly for current sharing [15]. In I–V droop mechanism, output dc voltage as global indicator is the key information which is supposed to be the same at each point

along the droop-based dc MGs. However, the mismatched networks make the assumption untenable and results in poor droop control performance on current sharing.

To enhance the accuracy of current sharing, several types of solutions have been proposed. In general, there are three basic methods to overcome the effect of mismatched networks on current sharing accuracy. The first method is based on the signal injection technique [16]. This approach can reduce the current sharing error by introducing the concept of 'frequency' into dc system. Here, the difference of frequency among DGs will cause a circulating small real power, according to which DG output voltage is adjusted, until the load current is shared properly. However, this approach increases the control system complexity and decreases the quality of the output voltage and current. The second method estimates the parameters of networks, which is then applied to set a virtual impedance to compensate voltage drops across the line resistance. In [17], the estimation strategy is dependent on the information during grid-connected mode, this means MGs can run in islanded mode only if it operates in grid-connected mode in advance. The voltage of common point is utilised in [18, 19] to simplify the estimation process; however, it may be impractical to obtain the information of common point especially in multi-bus networks [20, 21]. Resembling the control hierarchy of the traditional grid, the third method uses hierarchical structure consisting of three levels: primary, secondary, and tertiary control. In this hierarchical method, communication links are employed for accurate load current sharing. The primary control is usually designed with classic droop control to locally adjust the output voltage. To restore electrical parameters to their reference values, a secondary control is introduced. Conventionally, the secondary control is implemented in a centralised manner [22], which relies on an MG central controller sending compensation control messages to the DG local controller. Recently, secondary control has been embedded into the DG local controller in a distributed way, which employs low bandwidth communication to

exchange information with other DGs to tune the droop curve [23, 24]. Moreover, a sparse communication network is spanned across the MGs that enables limited messages passing among DGs, each DG only exchange data with its neighbours [25, 26]. In addition, economical operation and power flow optimisation are taken considerations into the tertiary control. Despite communication links are useful for accuracy of current sharing, it may cause new issues such as risk for lower reliability, scalability limitations and possible cost increments.

Responding to the concerns risen above, the implementation of dc MGs requires an efficient strategy to coordinate DGs without using communication links, information of network parameters or additional small signal. In essence, the 'modified global indicator' concept has been demonstrated to be effective for improving reactive power sharing in ac MGs, but only in typical structure with common bus [13, 14]. In this paper, we extend the application of such global indicator concept to dc MGs with multiple buses. Unlike most improved methods in dc MGs revolving around virtual resistance, this paper presents a series virtual capacitor for dc MGs (virtual capacitor concept in dc system was only applied for management of current ripple components [27], but not included the scope of current sharing). This virtual capacitor introduces a modified global indicator, change rate of dc output voltage $\dot{V}$, in order to eliminate the effect of mismatches in network. Moreover, to maintain the output voltage at steady state, a complementary voltage stabiliser with virtual resistance feature is developed. With effective shaping of virtual impedance, the current sharing accuracy can be improved. The operation under multiple dc-buses is also included in order to enhance the applicability of the proposed controller. The resulted solution features a fully decentralised framework in multi-bus dc MGs, which eliminates the need for communication links or dedicated central controller. The proposed control is model free, in the sense that it requires no knowledge of the dc MG topology or parameters such as transmission lines and load demands.

The rest of the work is outlined as follows. In Section 2, an overview of the multi-bus structure of a dc MG is presented along with an explanation of how network mismatches influence the traditional I–V droop performance on current sharing. Section 3 introduces the operation principle of the proposed control method and analyses the stability of the control system under different parameters variation. Simulation and experimental results obtained for verifying the control effectiveness and theoretical analysis are presented in Sections 4 and 5, before conclusions in Section 6.

2 DC MG structure and control

2.1 DC MG structure

Fig. 1 shows a typical dc MG system structure, in which DERs such as PV modules, wind turbines and energy storage system are decentralised connected to a common dc bus using interfacing converters. Due to increasing DGs and loads joining in, the configuration of dc MGs with multiple buses is emerging, as shown in Fig. 2. In this network, loads connecting straight to DGs are called as local loads, and the others are remote loads.

2.2 Modelling of dc MG with multiple buses

Compared with typical structure of dc MG with common dc bus, it is more difficult to assess or improve current sharing performance in multi-bus dc MG because of its complicated configuration. Solution for this issue is to develop a more comprehensive model for multi-bus dc MG. As shown in Fig. 2, the whole network can be regarded as a directed graph (digraph) $G = (v, \varepsilon)$. Such a graph is represented as a set of buses (nodes) v interconnected by a set of transmission lines (edges) ε. In this case, the network consists of m buses with DG as well as local load, n buses only with remote load and l transmission lines. For the purpose of study, we assume all lines and loads are resistive, and all the DGs have same
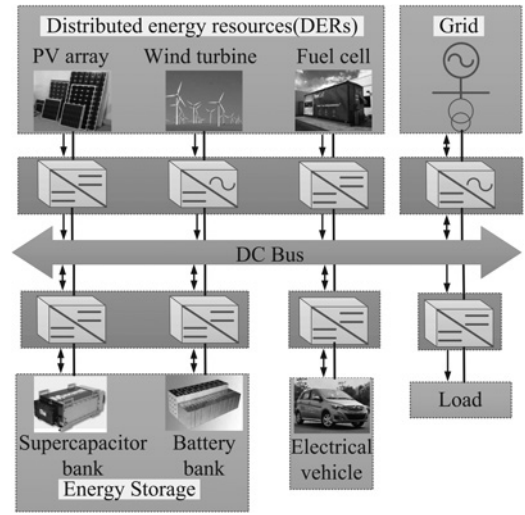

Fig. 1 *Typical structure of dc MG system with common bus*

current rating. The detailed models of each component and complete networks are derived hereinafter.

2.2.1 DG Model: Load current sharing control in dc microgrids can traditionally be realised by I–V droop mechanism, which is expressed as

$$u_{\mathrm{dc}i} = u_{\mathrm{dc}}^* - R_{\mathrm{d}}i_{\mathrm{dc}i}, \tag{1}$$

where u_{dc} is the converter dc output voltage, u_{dc}^* is the reference value of the dc output voltage, i_{dc} is the dc output current and R_{d} is the droop gain. DG based on traditional droop control can be regarded as series combination of a dc voltage source u_{dc}^* and a virtual resistance $\boldsymbol{R_{\mathrm{d}}}$.

Rewriting (1) in the matrix form by combining all the DGs equations together, the whole DGs model is given by

$$\boldsymbol{U}_{\mathrm{dc}} = u_{\mathrm{dc}}^* \mathbf{1}_{\boldsymbol{m}} - \boldsymbol{R_{\mathrm{d}}}\boldsymbol{I}_{\mathrm{dc}}, \tag{2}$$

where $\boldsymbol{U}_{\mathrm{dc}} = \begin{bmatrix} u_{\mathrm{dc}1} & u_{\mathrm{dc}2} & \cdots & u_{\mathrm{dc}m} \end{bmatrix}^{\mathrm{T}}$, $\boldsymbol{I}_{\mathrm{dc}} = \begin{bmatrix} i_{\mathrm{dc}1} & i_{\mathrm{dc}2} & \cdots & i_{\mathrm{dc}m} \end{bmatrix}^{\mathrm{T}}$, droop coefficient matrix $\boldsymbol{R_{\mathrm{d}}} = \mathrm{diag}(R_{\mathrm{d}})_{m \times m}$ and $\mathbf{1}_{\boldsymbol{m}}$ denotes a vector where all the m components equals one.

2.2.2 Transmission lines model: The voltage of transmission line k can be written as follows

$$u_{\mathrm{line}k} = R_{\mathrm{line}k}i_{\mathrm{line}k}. \tag{3}$$

In (3), $u_{\mathrm{line}k}$ and $i_{\mathrm{line}k}$ are the voltage and current of transmission line k, respectively; $R_{\mathrm{line}k}$ is the resistance value of line k. Hence the model of l transmission lines can be given by

$$\boldsymbol{U}_{\mathrm{line}} = \boldsymbol{R}_{\mathrm{line}}\boldsymbol{I}_{\mathrm{line}}, \tag{4}$$

where $\boldsymbol{U}_{\mathrm{line}} = \begin{bmatrix} u_{\mathrm{line}1} & u_{\mathrm{line}2} & \cdots & u_{\mathrm{line}l} \end{bmatrix}^{\mathrm{T}}$, $\boldsymbol{I}_{\mathrm{line}} = \begin{bmatrix} i_{\mathrm{line}1} & i_{\mathrm{line}2} & \cdots & i_{\mathrm{line}l} \end{bmatrix}^{\mathrm{T}}$ and line resistance matrix $\boldsymbol{R}_{\mathrm{line}} = \mathrm{diag}(R_{\mathrm{line}k})_{l \times l}$.

2.2.3 Loads model: For the m buses with DG, the model of whole local loads can be expressed as

$$\boldsymbol{I}_{\mathrm{LL}} = \boldsymbol{G}_{\mathrm{LL}}\boldsymbol{U}_{\mathrm{dc}}. \tag{5}$$

In (5), $\boldsymbol{I}_{\mathrm{LL}}$ represents current vector of local loads which is $\begin{bmatrix} i_{\mathrm{LL}1} & i_{\mathrm{LL}2} & \cdots & i_{\mathrm{LL}m} \end{bmatrix}^{\mathrm{T}}$, and $\boldsymbol{G}_{\mathrm{LL}} = \mathrm{diag}(g_{\mathrm{LL}i})_{m \times m}$ consists conductance value of each local load.
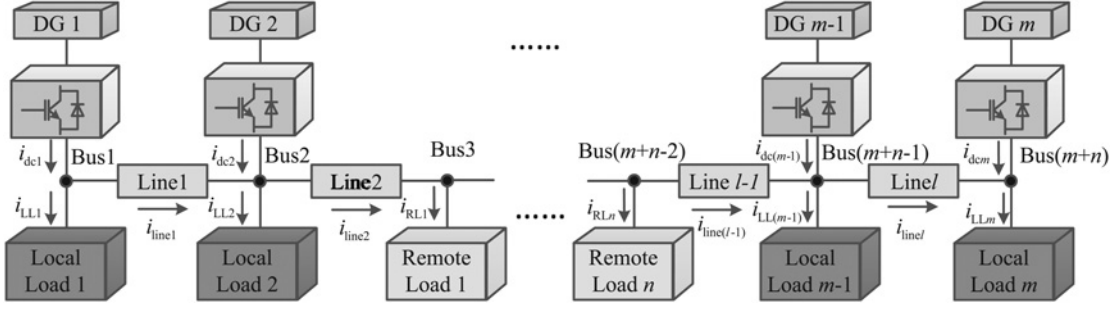
Fig. 2 *Dc MG system with multiple buses*

Likewise, the model of remote loads is also given by

$$I_{\mathbf{RL}} = G_{\mathbf{RL}}U_{\mathbf{RL}}, \tag{6}$$

where remote loads current vector $I_{\mathbf{RL}} = \begin{bmatrix} i_{\mathrm{RL}1} & i_{\mathrm{RL}2} & \cdots & i_{\mathrm{RL}n} \end{bmatrix}^{\mathrm{T}}$, corresponding voltage vector $U_{\mathbf{RL}} = \begin{bmatrix} u_{\mathrm{RL}1} & u_{\mathrm{RL}2} & \cdots & u_{\mathrm{RL}n} \end{bmatrix}^{\mathrm{T}}$ and remote loads conductance matrix $G_{\mathbf{RL}} = \mathrm{diag}(g_{\mathrm{RL}j})_{n \times n}$.

2.2.4 Complete network model: In the view of bus i, the network interconnection is expressed by Kirchhoff's current law (KCL) as follows

$$i_{\mathrm{S}i} - i_{\mathrm{L}i} = \sum_{k=1}^{l} a_{ik} i_{\mathrm{line}k}, \tag{7}$$

where $i_{\mathrm{S}i}$ represents output current of DG in bus i, $i_{\mathrm{L}i}$ is current of load at this bus and a_{ik} indicates the relationship between bus i and line k. a_{ik} will be $+1$ or -1 (depending on whether the line current is leaving or entering the bus) when line k is connected to bus i, else $a_{ik} = 0$. Hence, KCL in matrix form can be derived as

$$I_{\mathbf{S}} - I_{\mathbf{L}} = AI_{\mathbf{line}}, \tag{8}$$

where $I_{\mathbf{S}} = \begin{bmatrix} i_{\mathrm{S}1} & i_{\mathrm{S}2} & \cdots & i_{\mathrm{S}(m+n)} \end{bmatrix}^{\mathrm{T}}$, $I_{\mathbf{L}} = \begin{bmatrix} i_{\mathrm{L}1} & i_{\mathrm{L}2} & \cdots & i_{\mathrm{L}(m+n)} \end{bmatrix}^{\mathrm{T}}$ and A is the incidence matrix of $(m+n) \times l$ dimension.

On the other side, in the view of line k, the system can be expressed in matrix form by Kirchhoff's voltage law as follows

$$U_{\mathbf{line}} = A^{\mathrm{T}} U_{\mathbf{bus}}, \tag{9}$$

where bus voltage vector $U_{\mathbf{bus}} = \begin{bmatrix} u_{\mathrm{bus}1} & u_{\mathrm{bus}2} & \cdots & u_{\mathrm{bus}(m+n)} \end{bmatrix}^{\mathrm{T}}$.

Combining (4), (8) and (9), nodal voltage equation can be derived

$$I_{\mathbf{S}} - I_{\mathbf{L}} = A^{\mathrm{T}} R_{\mathbf{line}}^{-1} A U_{\mathbf{bus}} = G_{\mathbf{net}} U_{\mathbf{bus}}, \tag{10}$$

where nodal admittance matrix $G_{\mathbf{net}}$ is a Laplacian matrix with $(m+n) \times (m+n)$ dimension, which carries all the details of the multi-bus network.

According to classifications of loads, the vectors of each bus can be revised as

$$I_{\mathbf{S}} = \begin{bmatrix} I_{\mathrm{dc}} \\ 0_n \end{bmatrix}, \quad I_{\mathbf{L}} = \begin{bmatrix} I_{\mathrm{LL}} \\ I_{\mathrm{RL}} \end{bmatrix}, \quad U_{\mathbf{bus}} = \begin{bmatrix} U_{\mathrm{dc}} \\ U_{\mathrm{RL}} \end{bmatrix}, \tag{11}$$

where 0_n is a null vector with n elements.

Hence, nodal voltage equation (10) can be rewritten as

$$\begin{bmatrix} I_{\mathrm{dc}} - I_{\mathrm{LL}} \\ -I_{\mathrm{RL}} \end{bmatrix} = \begin{bmatrix} G_{\mathbf{net}1} & G_{\mathbf{net}2} \\ G_{\mathbf{net}2}^{T} & G_{\mathbf{net}3} \end{bmatrix} \begin{bmatrix} U_{\mathrm{dc}} \\ U_{\mathrm{RL}} \end{bmatrix}, \tag{12}$$

where $G_{\mathbf{net}1}$ and $G_{\mathbf{net}3}$ are nodal admittance matrix among buses with local loads and among buses with remote loads, respectively. $G_{\mathbf{net}2}$

represents interconnection relationship from buses with local loads to buses with remote loads.

Combining (5) (6) and (12), relationship between DG output current and output voltage can be derived

$$I_{\mathbf{dc}} = (G_{\mathbf{net}1} + G_{\mathbf{LL}} - G_{\mathbf{net}2}(G_{\mathbf{RL}} + G_{\mathbf{net}3})^{-1} G_{\mathbf{net}2}^{\mathrm{T}}) U_{\mathbf{dc}}. \tag{13}$$

Considering all DGs adopting traditional I–V droop control, by substituting (2) in (13), following equation can be obtained

$$I_{\mathbf{dc}} = C u_{\mathrm{dc}}^{*} 1_m, \tag{14}$$

where $C = (E + BR_{\mathbf{d}})^{-1} B$ and $B = G_{\mathbf{net}1} + G_{\mathbf{LL}} - G_{\mathbf{net}2}(G_{\mathbf{RL}} + G_{\mathbf{net}3})^{-1} G_{\mathbf{net}2}^{\mathrm{T}}$, E is identity matrix. For ith DG, the output current relationship of each DG can expressed as

$$i_{\mathrm{dc}i} = d_i u_{\mathrm{dc}}^{*}, \tag{15}$$

where $d_i = \sum_{j=1}^{l} c_{ij}$.

For assessing the current sharing performance, the total current sharing error of system is defined as

$$\Delta I_{\mathrm{err}}\% = \frac{\sum_{i=1}^{m} |i_{\mathrm{dc}i} - i_{\mathrm{ave}}|}{\sum_{i=1}^{m} |i_{\mathrm{dc}i}|}, \tag{16}$$

where average current is $i_{\mathrm{ave}} = (\sum_{i=1}^{m} i_{\mathrm{dc}i})/m$.

The current sharing capability of traditional I–V droop control can be estimated by combining (15) and (16)

$$\Delta I_{\mathrm{err(I-V)}}\% = \sum_{i=1}^{m} \left| \frac{d_i}{\sum_{i=1}^{m} d_i} - \frac{1}{m} \right|. \tag{17}$$

From the modelling process of dc MGs with multiple buses, it can be realised that the performance of conventional droop control on current sharing is strongly influenced by the parameters of multi-bus networks, which is much more complicated than typical structure.

3 Operation principle of the proposed control method

In the traditional I–V droop control, the dc bus voltage plays an important role as a global indicator in decentralised control system of dc MGs. However, due to the complex structure of multi-bus networks, the output voltage of each DG can hardly be identical, which influences the performance of I–V droop on current sharing. To avoid this effect, this paper introduces a modified global indicator $\dot{V}$, change rate of the output voltage, to replace V in the traditional droop relationship. The proposed control method for current sharing is explained in this section.

3.1 Proposed improved droop control method

In ac MG, the reason why *P-f* droop can realise accurate power sharing performance is that the global indicator f (as change rate of power angle δ) is the same in whole system. In order to achieve current sharing in dc MGs, we also introduce change rate of output voltage as this global indicator. The proposed controller is expressed as (18), where m_{droop} is droop gain, and i_{dc}^* is the reference value of i_{dc} when $\dot{u}_{\text{dc}} = 0$.

$$\begin{cases} \dot{u}_{\text{dc}} = m_{\text{droop}}(i_{\text{dc}} - i_{\text{dc}}^*) \\ u_{\text{dc}} = u_{\text{dc}}^* + \int \dot{u}_{\text{dc}}\, dt \end{cases}. \tag{18}$$

The block diagram of (18) is shown in Fig. 3. Considering that all DGs have the same acceptable output voltage change rate value which belongs to the operational region $[-\dot{u}_{\text{dc-max}}, +\dot{u}_{\text{dc-max}}]$, therefore the negative and positive maximum acceptable value correspond to the situation when the output current equals to the rated value I_R and zero, respectively. Thus, the droop gain m_{droop} and initial condition of i_{dc}^* can be expressed as follows

$$m_{\text{droop}} = -\frac{2\dot{u}_{\text{dc-max}}}{I_R} \tag{19}$$

$$i_{\text{dc}}^*(0) = \frac{I_R}{2}. \tag{20}$$

To analyse voltage change rate of each DG, (13) can be used. Since load resistance is much larger than line resistances [28], the differential form of (13) can be expressed as

$$\dot{\boldsymbol{I}}_{\mathbf{dc}} = (\boldsymbol{G}_{\mathbf{net1}} - \boldsymbol{G}_{\mathbf{net2}}\boldsymbol{G}_{\mathbf{net3}}^{-1}\boldsymbol{G}_{\mathbf{net2}}^{\mathbf{T}})\dot{\boldsymbol{U}}_{\mathbf{dc}}. \tag{21}$$

As aforementioned, $(\boldsymbol{G}_{\mathbf{net1}} - \boldsymbol{G}_{\mathbf{net2}}\boldsymbol{G}_{\mathbf{net3}}^{-1}\boldsymbol{G}_{\mathbf{net2}}^{\mathbf{T}})$ is a Laplacian matrix, which means it has a zero eigenvalue associated with the eigenvector **1**. Considering the situation when all $\dot{u}_{\text{dc}}$ of each DG is the same, the relationship among change rate of output current can be expressed as (22), where $\boldsymbol{0}_m$ is null vector with m elements. This equation indicates that output current of each DG will keep unchanged when each $\dot{u}_{\text{dc}}$ is the same. Here, this situation is defined as steady state I.

$$\dot{\boldsymbol{I}}_{\mathbf{dc}} = \boldsymbol{0}_m. \tag{22}$$

Assuming at steady state I, change rate of each DG voltage is equal to $\dot{u}_{\text{ss}}$. Substituting $\dot{u}_{\text{ss}}$ into the proposed controller (18), the relationship among each DG's output current at steady state I can be obtained as (23), which shows that the load current is shared by each DG proportionally to their rated current.

$$\boldsymbol{I}_{\mathbf{dc}} = \left(\frac{\dot{u}_{\text{dc-max}} - \dot{u}_{\text{ss}}}{2\dot{u}_{\text{dc-max}}}\right)\boldsymbol{I}_R. \tag{23}$$

Fig. 4 illustrates the operation of the proposed method considering any two DGs as per Fig. 2. Assuming the system is already steady before t_0, and current of DGs are $\text{DG}_i(i_{\text{dc}i}(t_0))$ and $\text{DG}_j(i_{\text{dc}j}(t_0))$. As load k (which is located closer to DG_j hypothetically) increases at a certain moment, the output current of $\text{DG}_j(i_{\text{dc}j}(t_1))$ increases more drastically than $\text{DG}_i(i_{\text{dc}i}(t_1))$ to pick up the load. According to the proposed droop curve, the relationship between the change rate of output voltage can be expressed as $\dot{u}_{\text{dc}j}(t_1) < \dot{u}_{\text{dc}i}(t_1)$, which
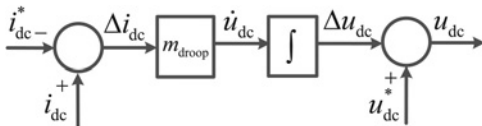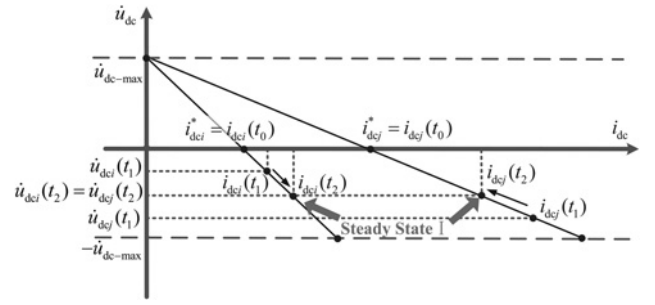

Fig. 4 *Principle of proposed droop controller*

means the output voltage of DG_j decreases more quickly than DG_i, and the load current flows from DG_j to DG_i gradually in this process. Eventually, $\dot{u}_{\text{dc}i}(t_2)$ and $\dot{u}_{\text{dc}j}(t_2)$ become the same and output current of each DGs keeps unchanged, the system arrives at steady state I.

From dc MG perspective, conventional droop mechanism has an inherent series virtual resistance. To investigate the virtual impedance characteristic of the proposed method, the variation of controller equation (18) can be expressed as

$$i_{\text{dc}} = i_{\text{dc}}^*(0) + \frac{\dot{u}_{\text{dc}}}{m_{\text{droop}}}. \tag{24}$$

In (24), the output current of DG is sum of initial current reference $i_{\text{dc}}^*(0)$ and item proportional to change rate of voltage. The first addend can be regard as a current source, while the second addend is equivalent to a virtual capacitor C_v whose value is $-1/m_{\text{droop}}$. The equivalent circuit of DG adopting proposed droop control is shown in Fig. 5. Here, this virtual capacitor introduces global indicator $\dot{V}$ into dc MG for achieving accurate current sharing. However, there will be current flowing through virtual capacitor while DG current i_{dc} is not equal to $i_{\text{dc}}^*(0)$, which would keep voltage changing even system operating in steady state I. Solution for this problem will be discussed in next subsection.

The following accounts can be taken in order to consider bidirectional power flow. As current constrain enlarges in bidirectional mode, operational region $[-I_R, +I_R]$ is substituted in proposed controller and the resulting parameters are modified as follows to obtain bidirectional power flow capability.

$$m_{\text{droop(bi)}} = -\frac{\dot{u}_{\text{dc-max}}}{I_R} \tag{25}$$

$$i_{\text{dc}}^*(0)_{\text{(bi)}} = 0. \tag{26}$$

3.2 Complementary voltage stabiliser

As shown in Fig. 4, the change rate of output voltage of each DG is the same $(\dot{u}_{\text{dc}i}(t_2) = \dot{u}_{\text{dc}j}(t_2))$ at steady state I, however, they do not equal to zero which results in output voltage still varying.
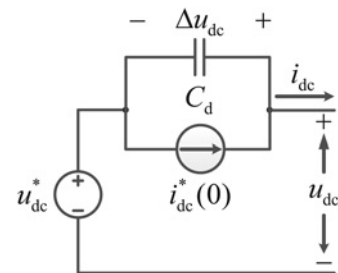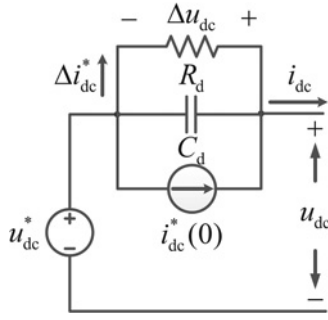

Fig. 3 *Block diagram of proposed droop controller*

Fig. 5 *Equivalent circuit of DG adopting proposed droop control*

Fig. 6 *Equivalent circuit of DG combining proposed droop control and voltage stabiliser*

Fig. 8 *Principle of voltage stabiliser*

Therefore, a complementary voltage stabiliser is proposed to keep output voltage unchanged.

As analysed in Section 3.1, the reason why voltage keeps changing is because there is still current flowing through virtual capacitor. Hence, the key idea of designing voltage stabiliser is adding a shunt virtual resistance R_v to cover the current difference $(i_{dc} - i_{dc}^*(0))$, which is shown in Fig. 6.

Combining with complementary voltage stabiliser, (24) can be rewritten as

$$i_{dc} = i_{dc}^*(0) + \frac{\dot{u}_{dc}}{m_{droop}} + \Delta i_{dc}^*. \qquad (27)$$

where complementary voltage stabiliser can be expressed as

$$\Delta i_{dc}^* = \frac{\int \dot{u}_{dc}\, dt}{-R_v}. \qquad (28)$$

Compared with hierarchical control in dc MG, this voltage stabiliser with integral feature can be seen as secondary control used for compensating steady state error ($\dot{u}_{dc}$) produced by primary control. However, unlike conventional secondary control, this $\dot{u}_{dc}$ decay process is implemented in fully decentralised fashion. Define $\tau = R_v C_v$, which stands for the time constant in the decay process. It is worth mentioning that the decay time constant τ of all DGs should be identical to make sure $\dot{u}_{dc}$ of each DG keeps at the same pace in this process.

The control block diagram of voltage stabiliser is shown in Fig. 7, and the operation of voltage stabiliser is illustrated in Fig. 8. At t_2 moment, system arrives at steady state I, but change rate of output voltage of each DG does not equal to zero. According to (28), the voltage stabiliser will shift the proposed droop curve by generating an increment of i_{dc}^* which will force $\dot{u}_{dc}$ towards to zero. At t_3 moment, change rate of output voltage becomes zero $\dot{u}_{dc}(t_3) = 0$ and output voltage maintains stable, the system arrives at steady state II.

3.3 Analysis of the proposed current sharing control system

As analysed above, the proposed current sharing control system consists of two parts. The first part is droop controller which introduces a new global indicator by adopting a virtual capacitor for improving current sharing accuracy. The second part is the complementary voltage stabiliser which pushes change rate of output voltage towards zero by adding a virtual shunt resistance. The overall control block diagram is shown in Fig. 9, where
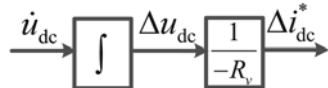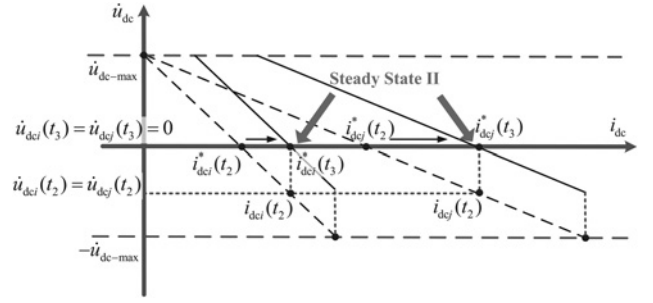

Fig. 7 *Block diagram of voltage stabiliser*

voltage stabiliser and proposed droop controller can be seen as outer loop controller and inner loop controller, respectively, and reference of current reference value i_{dc}^* is the interface between the two control loops.

Theoretically, the proposed control system can achieve the current sharing perfectly if the time constant of the outer loop (τ) is enough longer than the one associated with the inner loop. But in practical application, selecting value of τ need to consider the output voltage deviation. For that reason, the following procedure is developed to define the limits of τ. Here, (18), (28) and Fig. 9 are used to express the output voltage deviation as

$$\Delta u_{dc}(s) = K_{DC} \cdot G_d(S) \cdot (i_{dc}(s) - i_{dc}^*(0)) \qquad (29)$$

where $K_{DC} = \tau m_{droop}$, $G_d(S) = 1/(\tau s + 1)$.

Equation (29) shows that deviation of output voltage results from the current difference going through a low pass filter $G_d(S)$ and dc gain K_{DC}. The longer decay time constant τ is, the more accurate current sharing can be achieved, but on the other hand, the larger voltage deviation happens. To guarantee that the voltage deviation does not exceed its maximum acceptable value, the value of the decay time constant should be limited according to (19), (20) and (29).

$$\tau \leq \frac{\Delta u_{dc\text{-}max}}{\dot{u}_{dc\text{-}max}}. \qquad (30)$$

From the virtual impedance perspective, small virtual resistance can pick up current difference $(i_{dc} - i_{dc}^*(0))$ easily and shorten the time of $\dot{u}_{dc}$ decay process, but the performance of virtual capacitor will be influenced. Conversely, large value virtual resistance can guarantee sharing accuracy, but would cause large voltage deviation accordingly.
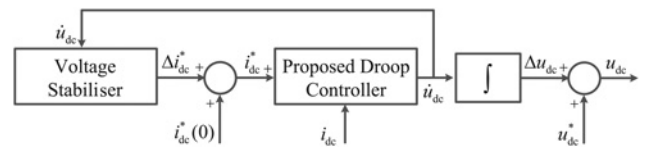

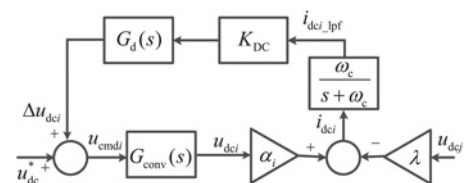Fig. 9 *Overall control block diagram of proposed current sharing control*

Fig. 10 *Detailed model of control diagram for stability analysis*

Table 1 System parameters used in stability analysis

Item	Value	Unit
R_{RL}	30	Ω
$R_{line i}$	2.9	Ω
$R_{line j}$	1.4	Ω
m_{droop}	-1–-100	V/A s
τ	0.5–10	s^{-1}
ω_c	10–200	rad/s

Table 2 Multi-bus networks parameters

Item	Value	Unit
R_{LL1}	95	Ω
R_{LL2}	80	Ω
R_{RL1}	100–300	Ω
R_{LL3}	65	Ω
R_{LL4}	50	Ω
R_{line1}	1	Ω
R_{line2}	2	Ω
R_{line3}	2	Ω
R_{line4}	1	Ω

Table 3 Electrical and control parameters for DGs

Item	Value	Unit
u_{dc}^*	150	V
V_{in}	90	V
capacitor	2.2	mF
inductance	2	mH
I_R	3	A
R_d	5	Ω
m_{droop}	-8	V/A s
τ	3	s^{-1}
ω_c	126	rad/s

To have a better evaluation of the proposed control method, system stability is analysed for any two DGs (DG$_i$ and DG$_j$) in dc MG shown in Fig. 2. The system can be equivalently changed to DGs connected to remote load through transmission lines by using Δ-Y transformation [29]. Thus, the detailed model of control diagram for i_{th} DG can be shown in Fig. 10, where system configuration parameters α_i, α_j and λ are expressed as

$$
\begin{cases}
\alpha_i = \dfrac{R_{line j} + R_{RL}}{R_{line i} \cdot R_{line j} + R_{line i} \cdot R_{RL} + R_{line j} \cdot R_{RL}} \\
\alpha_j = \dfrac{R_{line i} + R_{RL}}{R_{line i} \cdot R_{line j} + R_{line i} \cdot R_{RL} + R_{line j} \cdot R_{RL}} \\
\lambda = \dfrac{R_{RL}}{R_{line i} \cdot R_{line j} + R_{line i} \cdot R_{RL} + R_{line j} \cdot R_{RL}}
\end{cases} \quad (31)
$$

From Fig. 10, the output voltage of each DG can be derived as

$$
\begin{cases}
u_{dci}(s) = G_{conv}(s)\left[\dot{u}_{dc}^* + K_{DC}G_d(S)\dfrac{\omega_c}{s+\omega_c}(\alpha_i u_{dci} - \lambda u_{dcj})\right] \\
u_{dcj}(s) = G_{conv}(s)\left[u_{dc}^* + K_{DC}G_d(S)\dfrac{\omega_c}{s+\omega_c}(\alpha_j u_{dcj} - \lambda u_{dci})\right]
\end{cases} \quad (32)
$$

where ω_c is the cutting frequency of the low pass filter for output current, the voltage loop $G_{conv}(s) \simeq 1$ [30].

By combining (29), (31) and (32), the system characteristic equation can be obtained as

$$ As^4 + Bs^3 + Cs^2 + Ds + E = 0 \quad (33) $$

where

$$
\begin{cases}
A = \tau^2 \\
B = (2\tau + 2\tau^2 \omega_c) \\
C = [1 + 4\tau\omega_c + \tau^2\omega_c^2 - (\alpha_1 + \alpha_2)(\tau^2\omega_c m_{droop})] \\
D = [2\omega_c + 2\omega_c^2\tau - (\alpha_1 + \alpha_2)(\tau\omega_c m_{droop})(\tau\omega_c + 1)] \\
E = [\omega_c^2 - (\alpha_1 + \alpha_2)(\tau^2\omega_c m_{droop}) + (\tau\omega_c m_{droop})(\alpha_1\alpha_2 - \lambda^2)]
\end{cases} \quad .
$$
$$ (34) $$
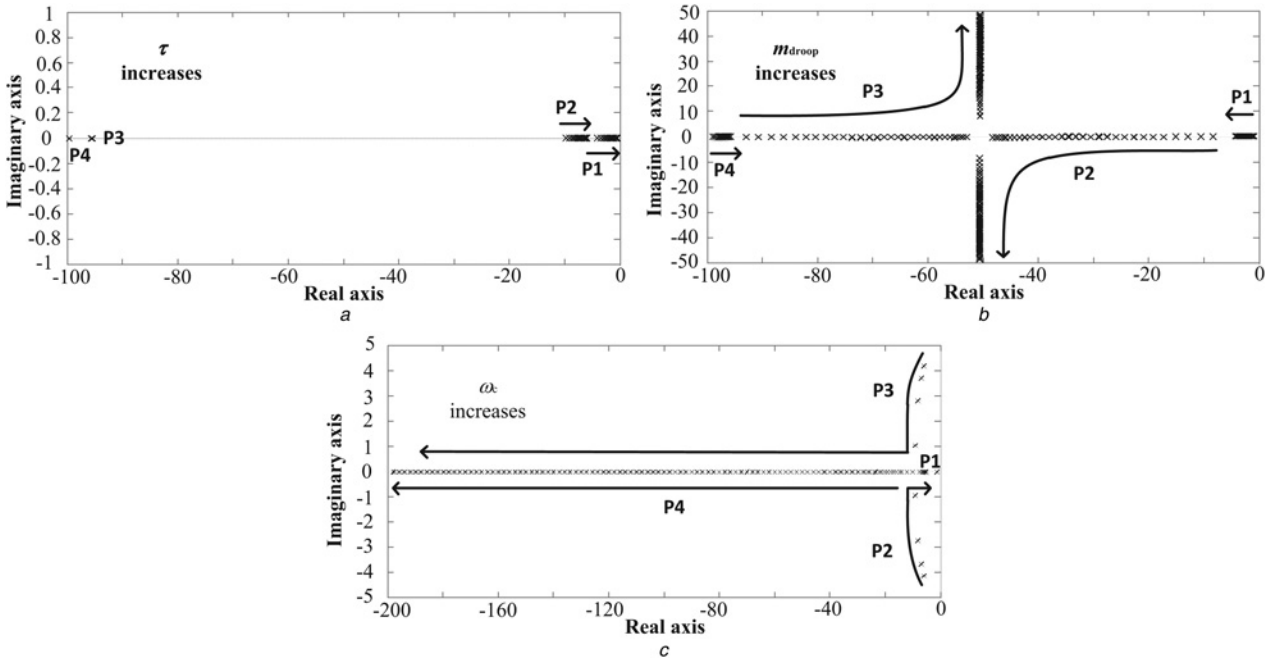
Fig. 11 Root locus diagrams of proposed control with variations of different parameters
a decay time constant increases
b droop gain increases
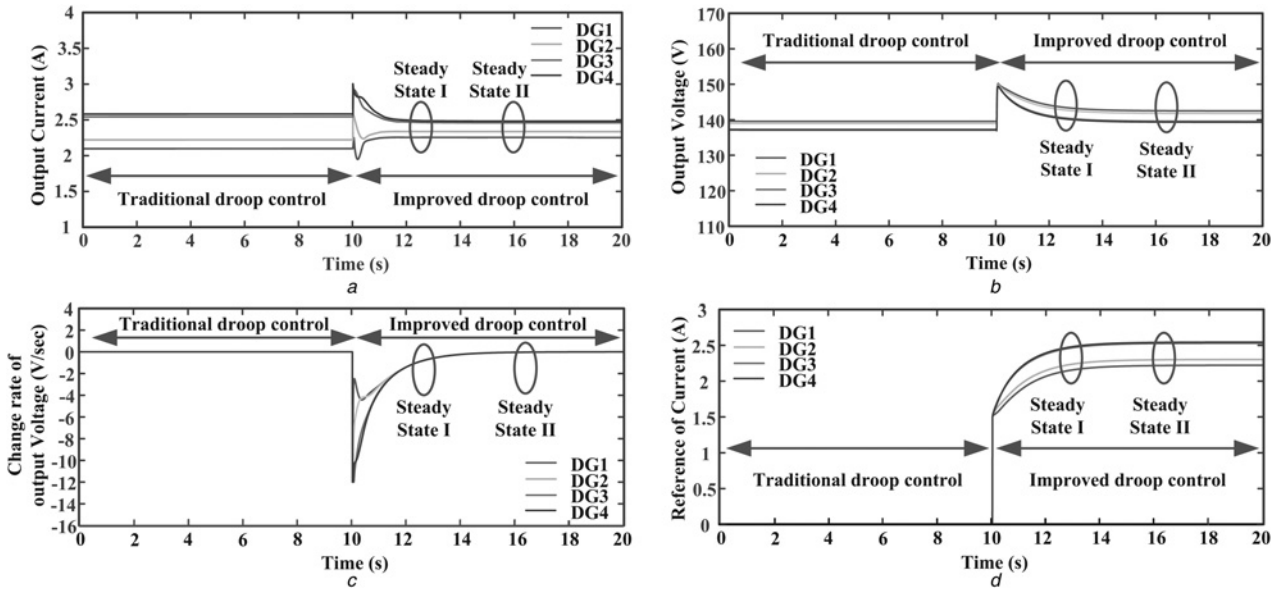*c* cutting frequency increases

Fig. 12 *Comparison of simulation results between traditional droop control and improved droop control*

a output current
b output voltage
c change rate of output voltage
d reference of current

The stability of the closed-loop can be tested by analysing the location of the dominant closed-loop of (34) while varying the decay time constant τ, the proposed droop gain m_{droop} and cutting frequency ω_c. The detailed parameters are listed in Table 1. The root locus diagrams with different decay time constant, droop gain and cutting frequency are shown in Figs. 11*a–c* respectively. From Figs. 11*a–c*, it is indicated that system stability can be ensured because all the poles are located on the left half plane.
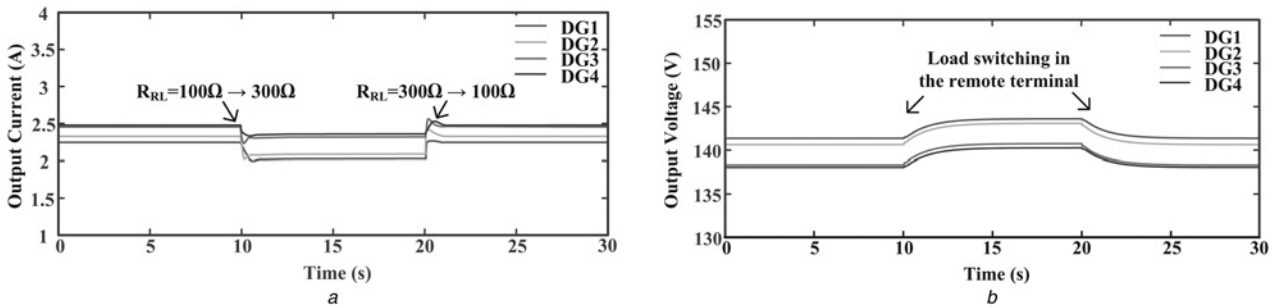

Fig. 13 *Simulation results during load switching with proposed control*
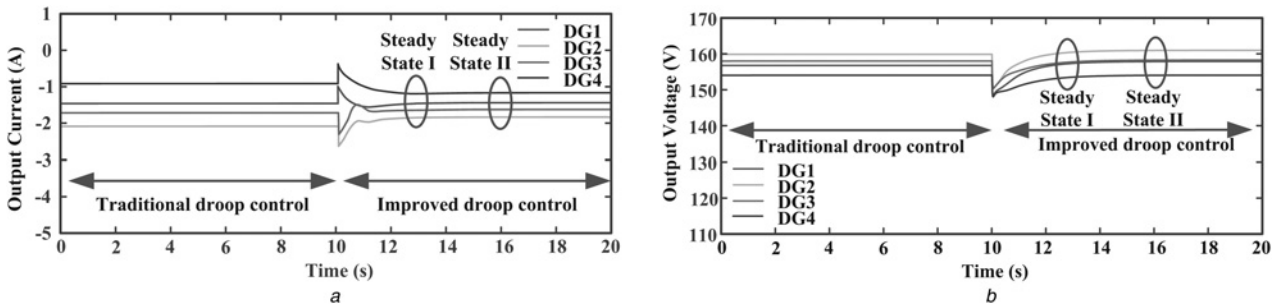*a* output current
b output voltage

Fig. 14 *Comparison of simulation results between traditional droop control and improved droop control in bidirectional mode*
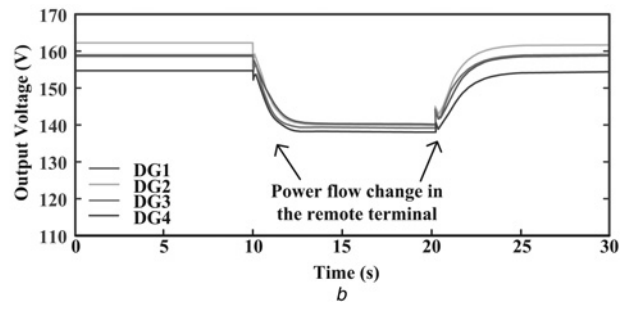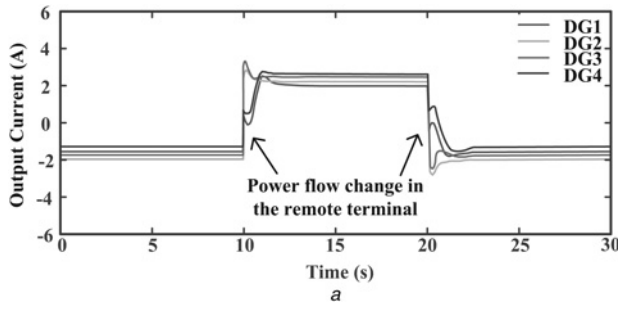*a* output current
b output voltage

Fig. 15 *Simulation studies on bidirectional performance of proposed control in a case of load change*
a output current
b output voltage

4 Simulation results

This section presents the simulation results to test the effectiveness and performance of the proposed control. The multi-bus dc MG system depicted in Fig. 2 is built in Plecs/Matlab. The detailed information of this multi-bus is listed in Table 2, while the electrical and control parameters of DGs are given in Table 3.

4.1 Comparative studies of traditional droop controller versus proposed controller

Fig. 12 presents a comparative simulation results between traditional controller and proposed controller. Each DG in this MG is initially controlled by the traditional I–V droop. At this stage ($t = 0$ s–10 s), existence of line resistance values and a wide local load variety cause several mismatches, which makes DG output voltage hardly be the same. This effect produces a high current sharing error $\Delta I_{err}\% = 8.47\%$. From $t = 10$ s, the proposed controller starts to govern the dc MG system. Here, by means of the virtual capacitor, the controller inserts the change rate of output voltage to be the new global indicator, which is less influenced by mismatched parameters in the dc MG. At $t = 13$ s, the change rate of output voltages become the same, which implies output current will keep unchanged and system arrives at steady state I. As voltage deviation Δu_{dc} increases, the current flowing through virtual resistance grows and offsets current in virtual capacitor gradually, which results in change rate of output voltage decaying. At $t = 16$ s, the change rates of output voltage become zero and the system arrives at steady state II. As a result, current sharing accuracy is finally achieved and $\Delta I_{err}\%$ is decreased to 4.22%. It is worth to note that, as analysed in Section 3.3, the load current cannot be shared perfectly because of selection limit of τ.

4.2 Load switching performance

The proposed controller performance in case of load switching is shown in Fig. 13. The remote load R_{RL1} at bus 3 is changed in step between 100 to 300 Ω in this figure, where fast current sharing and stable regulation can be observed.

4.3 Bidirectional power flow performance

As analysed in Section 3.1, bidirectional power flow capability can be obtained as current constraints extends to $[-I_R, +I_R]$ and $m_{droop}, i_{dc}^*(0)$ changes accordingly. Fig. 14 presents a comparative simulation results between traditional controller and proposed control when 3 kW active power is injected into the remote terminal. The current sharing accuracy is improved and the error of sharing $\Delta I_{err}\%$ is reduced from 22.0 to 11.6%. Fig. 15 shows the controller performance in case of load switching, the power injected in remote terminal is changed in step between 0 to 3 kW in this figure, where fast and stable operation is achieved in bidirectional mode.

5 Experimental validation

To validate the feasibility of the proposed current sharing method, a dc MG laboratory setup with two identical DGs that use boost dc–dc converters was built as shown in Fig. 16. The networks structure and parameters can be referred to Table 1. Matlab/Simunlink has been used for implementation of the DG control system. To control in real time, the code was compiled using a dSPACE 1104, while the pulse width modulation signals were generated with 10 kHz carriers in an integrated FPGA DS5203. Electrical and controller parameters of DG are listed in Table 3.

Figs. 17*a–d* show the experimental results of output current i_{dc}, output voltage u_{dc}, change rate of voltage $\dot{u}_{dc}$ and current reference value i_{dc}^*, respectively. For convenient comparison and analysis, traditional control is used before $t = 10$ s, and after $t = 10$ s proposed control is adopted instead.
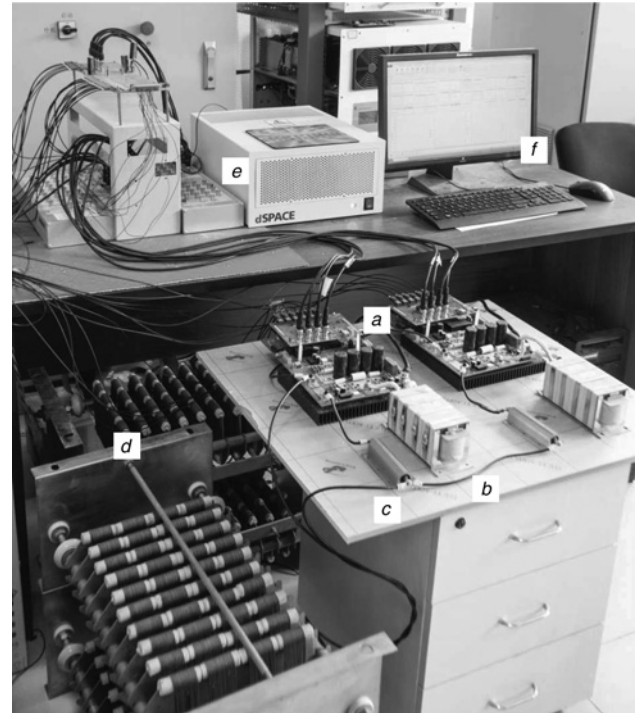

Fig. 16 *Laboratory prototype*

a Boost dc–dc converters
b Converter inductances
c Transmission lines
d Resistive loads
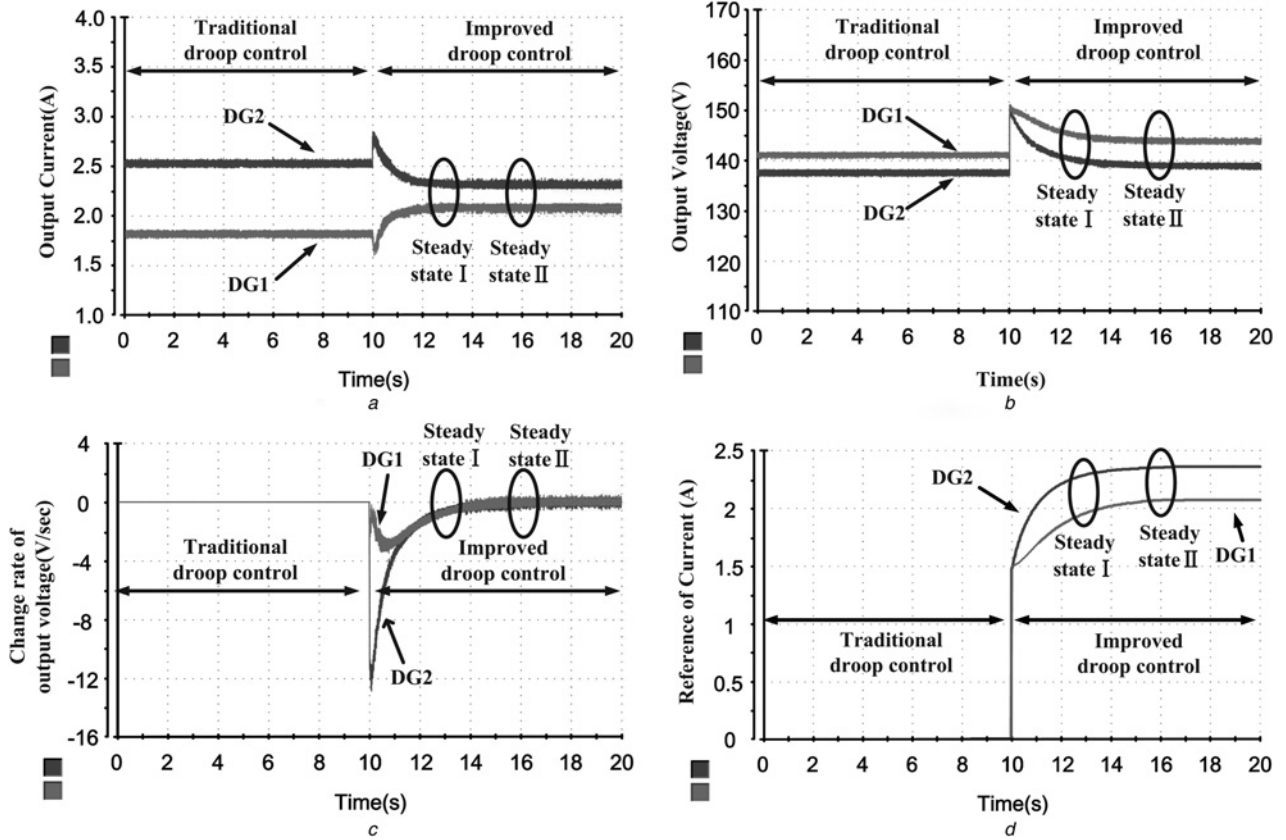*e* dSPACE1104
f Monitoring PC with control desk

Fig. 17 *Comparison of experimental results between traditional droop control and improved droop control*

a output current
b output voltage
c change rate of output voltage
d reference of current

i. 0–10 s

As analysed in Section 2.2, mismatched networks has negative impact on current sharing performance of traditional droop control.

ii. 10–13 s

As analysed in Section 3.1, due to $R_{\text{line2}} < R_{\text{line1}}$ much more load current is allocated to DG_2 (shown in Fig. 17a), whose change rate of output voltage is more negative than DG_1 according to the proposed droop curve Fig. 17c, hence the output voltage of DG_2 will decrease faster Fig. 17b and load current flows from DG_2 to DG_1 which helps improve the accuracy of current sharing. At $t = 13$ s the change rate of output voltages become the same and output currents keep unchanged, system arrives at steady state I.

iii. 13–16 s

As analysed in Section 3.2, the proposed droop curve shifts to the right since the current references of two DGs increased Fig. 17d, and the change rates of the output voltage decay at same pace Fig. 17c. At $t = 16$ s the change rates of output voltage become zero and output voltages keep unchanged, system arrives at steady state II. It is worth mentioning that the output currents keep unchanged Fig. 17a in the whole voltage stabiliser process.

In terms of current sharing error of system, the traditional I–V droop control yields to $\Delta I_{\text{err}}\% = 28.6\%$ due to mismatch in network, while the proposed control gives $\Delta I_{\text{err}}\% = 10.3\%$. Clearly, the proposed method employing a global indicator $\dot{V}$ provides improved current sharing accuracy. Figs. 18a–d show the experimental results during load switching with proposed control. At $t = 10$ s load switching happens, much more load current is allocated to DG_2 Fig. 18a, whose change rate of output voltage is more negative than DG_1 according to the proposed droop curve Fig. 18c, hence the output voltage of DG_2 will decrease faster Fig. 18b and load current flows from DG_2 to DG_1. At $t = 13$ s the

change rate of output voltages become the same and output currents keep unchanged, system arrives at steady state I. Current references of two DGs increased Fig. 18d, and the change rates of the output voltage decay at same pace Fig. 18c. At $t = 16$ s the output voltage change rates become zero and output voltages keep unchanged while system arrives at steady state II. As shown in Fig. 18, the proposed control performs fast current sharing and stable operation.

6 Conclusion

A decentralised control method for dc MGs under multiple dc-buses has been presented and analysed in this paper. The proposed controller makes use of the 'modified global indicator' concept in its formulation in order to provide an improved current sharing accuracy. To achieve this, a virtual capacitor representation has been addressed in order to introduce the change rate of the dc output voltage. This global indicator has been employed to avoid negative effect on current sharing caused by mismatched networks. A complementary virtual resistance has been added for keeping output voltage at steady state. Alongside the advantages of communication links, dedicated central controller or knowledge of networks are not needed, the proposed controller keeps the decentralised characteristics. The performance of the proposed control method considering line resistance variations and the filter dynamics was investigated by eigenvalue analysis. This analysis have shown that the proposed controller ensure small-signal stability. In addition, simulation and experimental results clearly showed that implementation of the proposed controller behaves accurately and fast during load changes.
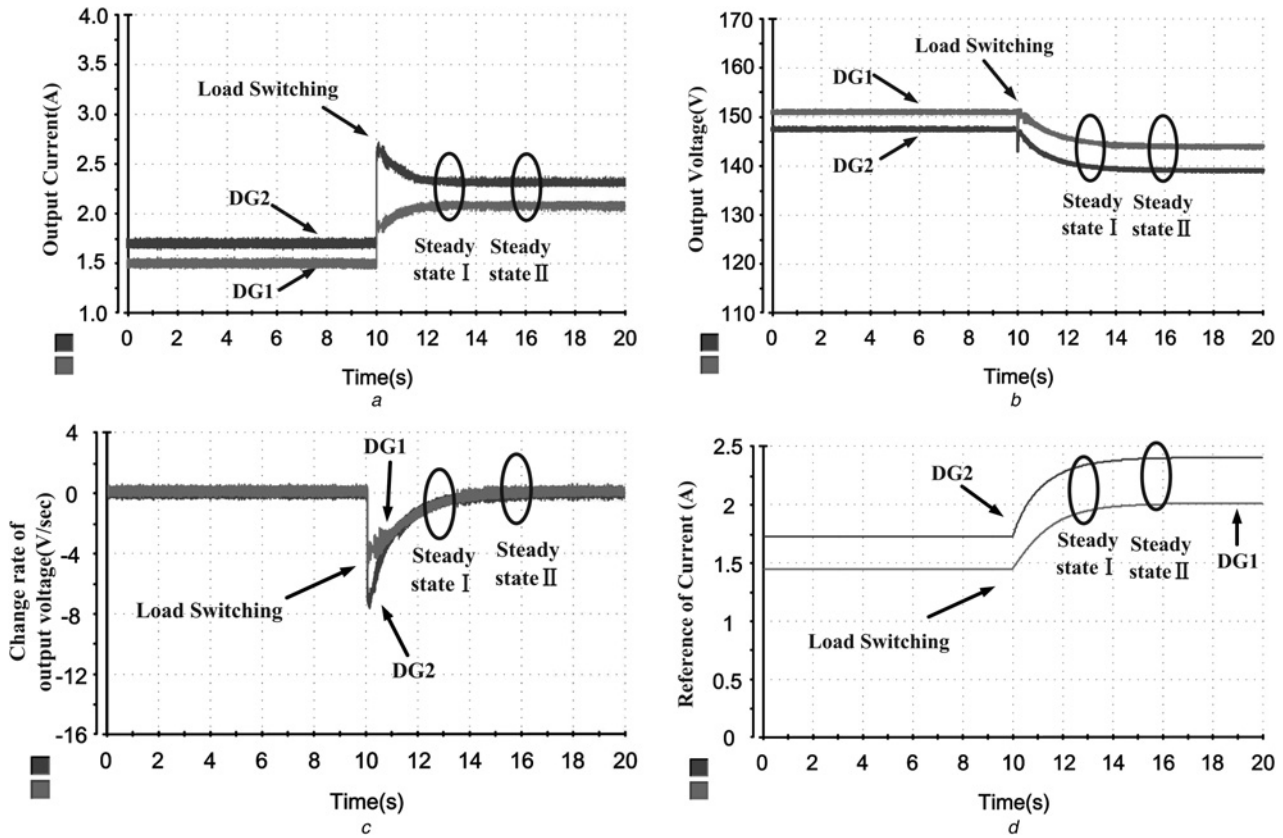
Fig. 18 *Experimental results during load switching with proposed control*
a output current
b output voltage
c change rate of output voltage
d reference of current

7 Acknowledgment

This research is supported by 'Application Technology Research and Engineering Demonstration Program of National Energy: Research on Generic Technology of Active Distribution Network Based on Hierarchical Energy Storage' of China (Grant No: NY20150301).

8 References

1 Lasseter, R.: 'Microgrids'. IEEE Power Engineering Society Winter Meeting, 2002, New York, US, January 2002, pp. 305–308
2 Wang, P., Jin, C., Zhu, D., *et al.*: 'Distributed control for autonomous operation of a three-port AC/DC/DS hybrid microgrid', *IEEE Trans. Ind. Electron.*, 2015, **2**, (62), pp. 1279–1290
3 Loh, P.C., Li, D., Chai, Y.K., *et al.*: 'Autonomous control of interlinking converter with energy storage in hybrid ac-dc microgrid', *IEEE Trans. Ind. Appl.*, 2013, **5**, (49), pp. 1374–1382
4 Ma, W.-J., Wang, J., Lu, X., *et al.*: 'Optimal operation mode selection for a dc microgrid', *IEEE Trans. Smart Grid*, 2016, Advance online publication, 2016, **PP**, (99), pp. 1–9
5 Khorsandi, A., Ashourloo, M., Mokhtari, H., *et al.*: 'Automatic droop control for a low voltage dc microgrid', *IET Gener. Transm. Distrib.*, 2016, **10**, (1), pp. 41–47
6 Kumar, M., Srivastava, S., Singh, S.: 'Control strategies of a dc microgrid for grid connected and islanded operations', *IEEE Trans. Smart Grid*, 2015, **7**, (6), pp. 1588–1601
7 Huang, P.-H., Liu, P.-C., Xiao, W., *et al.*: 'A novel droop-based average voltage sharing control strategy for dc microgrids', *IEEE Trans. Smart Grid*, 2015, **5**, (6), pp. 1096–1106
8 Xiao, J., Setyawan, L., Wang, P., *et al.*: 'Power-capacity-based bus-voltage region partition and online droop coefficient tuning for real-time operation of dc microgrids', *IEEE Trans. Energy Convers.*, 2015, **12**, (30), pp. 1338–1347
9 Sao, C., Lehn, P.: 'Control and power management of converter fed microgrids', *IEEE Trans. Power Syst.*, 2008, **8**, (23), pp. 1088–1098
10 Barklund, E., Pogaku, N., Prodanovic, M., *et al.*: 'Energy management in autonomous microgrid using stability-constrained droop control of inverters', *IEEE Trans. Power Electron.*, 2008, **9**, (23), pp. 2346–2352
11 Rokrok, E., Golshan, M.E.H.: 'Adaptive voltage droop scheme for voltage source converters in an islanded multibus microgrid', *IET Gener. Transm. Distrib.*, 2010, **5**, (4), pp. 562–578
12 Dou, C., Lv, M., Zhao, T., *et al.*: 'Decentralised coordinated control of microgrid based on multi-agent system', *IET Gener. Transm. Distrib.*, 2015, **9**, (16), pp. 2474–2484
13 Lee, C.T., Chu, C.C., Cheng, P.T.: 'A new droop control method for the autonomous operation of distributed energy resource interface converters', *IEEE Trans. Power Electron.*, 2013, **4**, (28), pp. 1980–1993
14 Sun, X., Hao, Y., Wu, Q., *et al.*: 'A multifunctional and wireless droop control for distributed energy storage units in Islanded AC microgrid applications', *IEEE Trans. Power Electron.*, Advance online publication, 2016, **PP**, (99), pp. 1–16
15 Li, C., Chaudhary, S.K., Savaghebi, M., *et al.*: 'Power flow analysis for low-voltage AC and DC microgrids considering droop control and virtual impedance', *IEEE Trans. Smart Grid*, Advance online publication, 2016, **PP**, (99), pp. 1–11
16 Tuladhar, A., Jin, K.: 'A novel control technique to operate dc/dc converters in parallel with no control interconnections'. 29th Annual IEEE Power Electronics Specialists Conf., 1998. PESC 98 Record. Fukuoka, Japan, May 1998, pp. 892–898
17 Khorsandi, A., Ashourloo, M., Mokhtari, H.: 'A decentralized control method for a low-voltage dc microgrid', *IEEE Trans. Energy Convers.*, 2014, **12**, (29), pp. 793–801
18 Sao, C., Lehn, P.: 'Autonomous load sharing of voltage source converters', *IEEE Trans. Power Deliv.*, 2005, **4**, (20), pp. 1009–1016
19 Zhong, Q.-C.: 'Robust droop controller for accurate proportional load sharing among inverters operated in parallel', *IEEE Trans. Ind. Electron.*, 2013, **4**, (60), pp. 1281–1290
20 Han, H., Liu, Y., Sun, Y., *et al.*: 'An improved droop control strategy for reactive power sharing in islanded microgrid', *IEEE Trans. Power Electron.*, 2015, **6**, (30), pp. 3133–3141
21 Bidram, A., Davoudi, A., Lewis, F.L., *et al.*: 'Secondary control of microgrids based on distributed cooperative control of multi-agent systems', *IET Gener. Transm. Distrib.*, 2013, **8**, (7), pp. 822–831
22 Guerrero, J., Vasquez, J., Matas, J., *et al.*: 'Hierarchical control of droop-controlled AC and DC microgrids-a general approach toward standardization', *IEEE Trans. Ind. Electron.*, 2011, **1**, (58), pp. 158–172
23 Lu, X., Guerrero, J., Sun, K., *et al.*: 'An improved droop control method for dc microgrids based on low bandwidth communication with dc bus voltage

restoration and enhanced current sharing accuracy', *IEEE Trans. Power Electron.*, 2014, **4**, (29), pp. 1800–1812

24 Anand, S., Fernandes, B.G., Guerrero, J.: 'Distributed control to ensure proportional load sharing and improve voltage regulation in low-voltage dc microgrids', *IEEE Trans. Power Electron.*, 2013, **4**, (28), pp. 1900–1913

25 Nasirian, V., Moayedi, S., Davoudi, A., *et al.*: 'Distributed cooperative control of dc microgrids', *IEEE Trans. Power Electron.*, 2015, **4**, (30), pp. 2288–2303

26 Morstyn, T., Hredzak, B., Agelidis, V.: 'Cooperative multi-agent control of heterogeneous storage devices distributed in a dc microgrid', *IEEE Trans. Power Syst.*, 2015, Advance online publication, 2015, **31**, (4), pp. 2974–2986

27 Cai, W., Liu, B., Duan, S., *et al.*: 'An active low-frequency ripple control method based on the virtual capacitor concept for BIPV systems', *IEEE Trans. Power Electron.*, 2014, **4**, (29), pp. 1733–1745

28 Augustine, S., Mishra, M., Lakshminarasamma, N.: 'Adaptive droop control strategy for load sharing and circulating current minimization in low-voltage standalone dc microgrid', *IEEE Trans. Sustain. Energy*, 2015, **1**, (6), pp. 132–141

29 Wang, P., Lu, X., Yang, X., *et al.*: 'An improved distributed secondary control method for DC microgrids with enhanced dynamic current sharing performance', *IEEE Trans. Power Electron.*, 2016, **9**, (31), pp. 6658–6673

30 Gu, Y., Xiang, X., Li, W., *et al.*: 'Mode-adaptive decentralized control for renewable dc microgrid with enhanced reliability and flexibility', *IEEE Trans. Power Electron.*, 2014, **9**, (29), pp. 5072–5080